Stem Cell Reports
Article
OPEN ACCESS

L-Proline Induces a Mesenchymal-like Invasive Program in Embryonic Stem Cells by Remodeling H3K9 and H3K36 Methylation

Stefania Comes,[1,2] Miriam Gagliardi,[2,6] Nicola Laprano,[1,2,6] Annalisa Fico,[1,2] Amelia Cimmino,[1,2] Andrea Palamidessi,[3] Dario De Cesare,[1,2] Sandro De Falco,[1,2] Claudia Angelini,[4] Giorgio Scita,[3,5] Eduardo J. Patriarca,[1,2] Maria R. Matarazzo,[2,*] and Gabriella Minchiotti[1,2,*]

[1]Stem Cell Fate Laboratory, Institute of Genetics and Biophysics "A. Buzzati-Traverso," CNR, 80131 Naples, Italy
[2]Institute of Genetics and Biophysics "A. Buzzati-Traverso," CNR, 80131 Naples, Italy
[3]IFOM, FIRC Institute of Molecular Oncology Foundation at IFOM-IEO Campus, 20139 Milan, Italy
[4]Institute for Applied Mathematics "Mauro Picone," CNR, 80131 Naples, Italy
[5]Dipartimento Scienze della Salute, San Paolo, Università di Milano, 20142 Milano, Italy
[6]These authors contributed equally to this work
*Correspondence: maria.matarazzo@igb.cnr.it (M.R.M.), gabriella.minchiotti@igb.cnr.it (G.M.)
http://dx.doi.org/10.1016/j.stemcr.2013.09.001

SUMMARY

Metabolites are emerging as key mediators of crosstalk between metabolic flux, cellular signaling, and epigenetic regulation of cell fate. We found that the nonessential amino acid L-proline (L-Pro) acts as a signaling molecule that promotes the conversion of embryonic stem cells into mesenchymal-like, spindle-shaped, highly motile, invasive pluripotent stem cells. This embryonic-stem-cell-to-mesenchymal-like transition (esMT) is accompanied by a genome-wide remodeling of the H3K9 and H3K36 methylation status. Consistently, L-Pro-induced esMT is fully reversible either after L-Pro withdrawal or by addition of ascorbic acid (vitamin C), which in turn reduces H3K9 and H3K36 methylation, promoting a mesenchymal-like-to-embryonic-stem-cell transition (MesT). These findings suggest that L-Pro, which is produced by proteolytic remodeling of the extracellular matrix, may act as a microenvironmental cue to control stem cell behavior.

INTRODUCTION

In recent years, a number of small molecules have been identified that control stem cell differentiation and/or cell reprogramming. Surprisingly, only a few metabolites have been identified in this context, possibly because their relevance has been underappreciated. The "physiological" compounds identified so far include epigenetic modifiers or regulators of the cell energy/redox status acting on mitochondrial oxidative metabolism. For example, saturated fatty acids and the acylcarnitines were shown to improve embryonic stem cell (ESC) differentiation (Yanes et al., 2010). Butyrate, a short-chain fatty acid, increases the efficiency of cell reprogramming by inhibiting histone deacetylases (Mali et al., 2010). Finally, ascorbic acid (vitamin C), a redox controller and a cofactor for histone demethylases, is a key regulator of stem cell differentiation and reprogramming (Cao et al., 2012; Esteban et al., 2010; Wang et al., 2011; Yang et al., 2008). However, it has recently become evident that also some naturally occurring amino acids can regulate stem cell behavior. Indeed, it has been shown that (1) ESC self-renewal depends on L-threonine catabolism (Shyh-Chang et al., 2013; Wang et al., 2009) and (2) L-proline (L-Pro) forces ESCs toward an epiblast stem cell (EpiSC)-like state (Washington et al., 2010) and regulates ESC metastability (Casalino et al., 2011). L-Pro is particularly interesting because its mitochondrial oxidative catabolism is linked to cell survival/cell death in cancer cells (Liu et al., 2012; Phang et al., 2012) and to life span extension in *C. elegans* (Zarse et al., 2012). Here, we provide evidence that physiological concentrations of L-Pro are sufficient to convert ESCs into mesenchymal-like, highly motile, invasive pluripotent stem cells, which acquire metastatic potential in vivo. This previously unforeseen embryonic-stem-cell-to-mesenchymal-like transition (esMT) is fully reversible either after L-Pro withdrawal or by addition of vitamin C. Most remarkably, L-Pro extensively remodels both the transcriptome and the epigenome, thus acting as a potent signaling metabolite in pluripotent stem cells.

RESULTS

L-Pro Modifies ESC Morphology Inducing Extensive Cytoskeletal Rearrangements

Mouse ESCs grow as leukemia inhibitory factor (LIF)-dependent flat colonies in the presence of L-Pro (Casalino et al., 2011; Washington et al., 2010). Examining different growth conditions, we found that this L-Pro-induced morphological transition markedly increased by lowering the cell-plating density to 50 ESCs/cm^2 (Figure S1 available online). Notably, clonal L-Pro-induced cell (PiC) colonies showed three distinctive zones (Figure 1A): (1) a "central

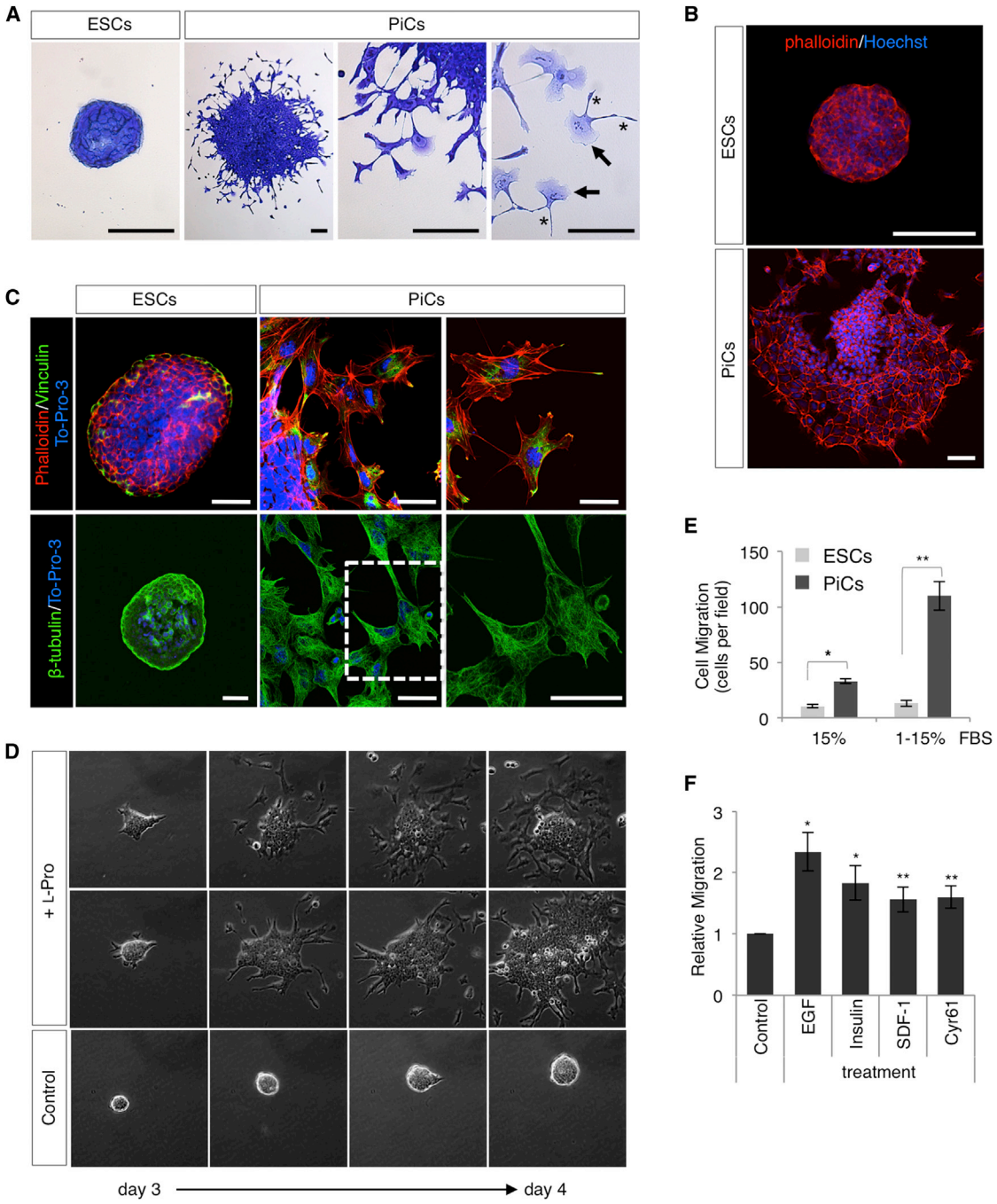

Figure 1. L-Pro Induces Cytoskeletal Rearrangements and Cell Motility in ESCs

(A and B) Representative photomicrographs of crystal violet (A) and Phalloidin-TRITC (B)-stained PiC and ESC colonies. Retraction fibers (*) and leading edge lamellipodia (arrow) are indicated (A). Nuclei were stained with Hoechst. (B) The scale bars represent 100 μm.

(C) Fluorescence confocal photomicrographs of ESCs/PiCs labeled for vinculin and phalloidin (upper panels) or for β-tubulin (lower panels). Actin stress fibers were labeled with Phalloidin-TRITC (red; [B and C]). Microtubules and focal adhesions were stained with anti-β-tubulin (green; [C], lower panels) and anti-Vinculin (green; [C], upper panels) antibodies. Nuclei were counterstained with TO-PRO-3. The scale bars represent 50 μm.

(D) Representative frames of time-lapse series from untreated (control) and L-Pro-treated ESCs. Images (20×) were captured starting from day 3 postplating.

(legend continued on next page)

zone" or "colony core" consisting of polygonal-shaped, tightly adherent cells; (2) a "peripheral zone" at the external margin of the colony, consisting of less-cohesive spindle-shaped cells; and (3) a "surrounding zone," forming a crown of mesenchymal-like cells scattered around the colony. These latter cells were characterized by a large nucleus with prominent nucleoli and a highly polarized mesenchymal shape with large and flat lamellipodial protrusions extending at the leading edge and needle-like trailing structures on the rear (Figure 1A). Alterations of cell shape and the formation of lamellipodial protrusions are primarily driven by actin cytoskeleton remodeling (Giannone et al., 2007; Ridley, 2011). Accordingly, we found that mesenchymal-like PiCs displayed long and polarized F-actin stress fibers frequently terminating in large and mature focal adhesion complexes. Presumably, as a consequence of this actin cytoskeleton-driven shape transition, also the microtubules organized into an extended network typical of mesenchymal motile cells (Figures 1B and 1C). Thus, ESCs undergo a morphological transformation, which is reminiscent of changes associated with the acquisition of persistent and directional cell locomotory properties.

L-Pro Induces a Motile Phenotype in ESCs

To test directly the possibility that L-Pro is sufficient to induce changes in adhesive and motile properties of stem cells, the ESC-to-PiC phenotypic transition was monitored by time-lapse video microscopy (Figure 1D; Movies S1, S2, and S3). Control ESCs formed compact colonies from which, occasionally, individual cells in direct contact with the substrate extended transient and short-lived cytoplasmic protrusions that appeared to direct the collective mode of locomotion of the entire colony (Movie S1). Cell divisions were visualized as transient swellings or "bubbles" that sporadically protruded from the colony. Within 1–3 days of plating, L-Pro-treated ESCs formed, as expected, spherical colonies; however, by day 3 onward, single, highly motile cells started to scatter, detaching from the colony margins through the extension of highly dynamic and prominent protrusions (Figure 1D; Movies S2 and S3). Importantly, these now freely motile, single PiCs maintained the ability to divide and frequently re-established dynamic and reversible cell-cell contacts with cells in the colony core. Consistent with the acquisition of directed cell motility, PiCs, but not ESCs, were able to migrate efficiently through porous membranes in transwell migration assays in response to gradients of fetal bovine serum (FBS) or toward different chemoattractants, including epidermal growth factor (EGF), insulin, stromal cell-derived factor-1 (SDF-1), and cysteine-rich angiogenic inducer 61 (Cyr61) (Figures 1E and 1F). Thus, L-Pro is sufficient to promote the transition of ESCs toward a motile mesenchymal-like phenotype.

L-Pro Induces Remodeling of the ESC Transcriptome

To elucidate whether a diverse transcriptional program is the basis of the morphological and motility differences between ESCs and PiCs, we compared their gene expression profiles. We found ~1,500 L-Pro-dependent, differentially regulated protein-coding genes (Figures 2A and 2B; Table S1). Gene ontology analysis revealed that L-Pro-regulated genes were functionally very diverse (Figure 2C), but the pluripotency-associated factors (*Oct4*, *Nanog*, and *Sox2*) remained, as expected, unchanged. Interestingly, whereas genes involved in L-Pro uptake (*Slc38a2*), synthesis (*Aldh18a* and *P5cr*), or catabolism (*Prodh*) were not affected (Table S1), both procollagen C-endopeptidase enhancer (*Pcolce*) and dipeptidyl peptidase 4 (*Dpp4/CD26)*, which regulate L-Pro recycling, were significantly downregulated. DPP4, which cleaves X-Pro dipeptides generating free L-Pro, was the most L-Pro-repressed protease (Table S1). In contrast, expression of the DPP4 inhibitor, glypican 3 (*Gpc3*), was induced. Thus, ESCs respond to increased extracellular levels of free L-Pro by repressing genes involved in L-Pro recycling. Remarkably, PiCs and EpiSCs (Brons et al., 2007; Tesar et al., 2007) shared 33% of differentially expressed protein-coding genes with respect to ESCs (Figure 2D). However, *Cer1*, *Asb4*, *Foxa2*, *Gata6*, *Sox17*, and *Stra8,* which are among the most upregulated genes in EpiSCs, did not change in PiCs. Similarly, the developmental pluripotency-associated genes *Dppa3, Dppa4*, and *Dppa5* that are repressed in EpiSCs were, instead, expressed at comparable levels in PiCs and ESCs (Brons et al., 2007; Tesar et al., 2007). Moreover, the transcription factor *Rex1* (*Zfp42*), which is silenced in epiblast cells just after implantation and is strongly repressed in EpiSCs, was only weakly downregulated in PiCs (Table S1). Notably, immunofluorescence analysis revealed that PiCs, like ESCs, were REX1 positive (≥95%) and that REX1 expression persisted in the mesenchymal-like PiCs scattered around the colony (Figures S2A and S2B). These data indicate that the morphological changes of PiCs are likely driven by a specific transcriptional program that is

(E) Average number of ESCs/PiCs migrating in 15% FBS (10.5 ± 1.5 ESCs versus 33 ± 3 PiCs) or toward a FBS gradient 1%–15% (13 ± 2 ESCs versus 110 ± 13 PiCs).
(F) Average number of PiCs migrating in 1% FBS either alone (control) or toward EGF (50 ng/ml), insulin (5 μg/ml), SDF-1 (100 ng/ml), or Cyr61 (200 ng/ml). Data are mean ± SD (n = 3); *p < 0.01; **p < 0.005.
See also Figure S1 and Movies S1, S2, and S3.

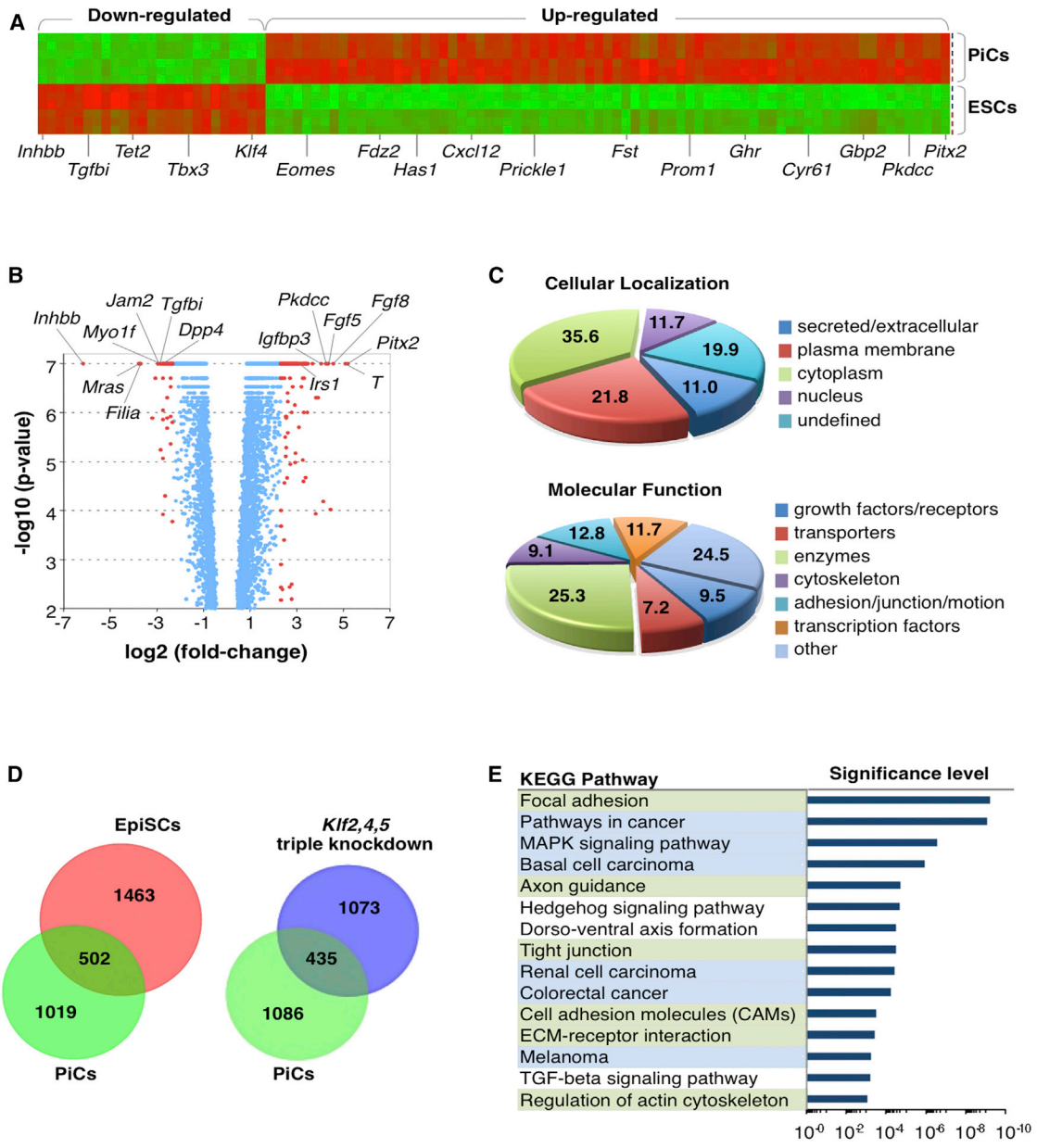

Figure 2. L-Pro Remodels the ESC Transcriptome

(A) Heat map diagram of differentially expressed genes in PiCs versus ESCs.

(B) Volcano plot showing the magnitude of differential expression [$\log_2$(fold change), x axis] compared to the measure of statistical significance [$-\log_{10}$(p value), y axis]. Genes with a magnitude of differential expression $\geq$5-fold are indicated in red.

(C) Gene ontology (GO) analysis (http://david.abcc.ncifcrf.gov). Pie chart showing the most represented GO term in the microarray analysis comparing PiCs versus ESCs. The numbers inside each pie slice show the fraction (%) of differentially expressed protein-coding genes (Table S1) in each category.

(D) Venn diagrams describing the overlap between genes differentially expressed in PiCs versus EpiSCs or *Klf2/Klf4/Klf5* (*Klf2,4,5*) triple knockdown ESCs compared with control ESCs.

(E) KEGG pathway enrichment analysis; pathways related to cytoskeleton/cell motility/adhesion or cancer are highlighted in green and blue, respectively.

See also Figure S2 and Table S1.

significantly different from the program induced in EpiSCs. Indeed, a significant set of genes regulated by L-Pro were either transcription factors or cofactors (~12%; Figure 2C; Table S1), among them several *K*rüppel-*l*ike *f*actors (*Klf*s), which are key regulators of cell differentiation and reprogramming. Of note, whereas *Klf2*, *Klf4*, and *Klf5* were all downregulated by L-Pro, the expression of *Klf6* and *Klf7* increased. Interestingly, PiCs and *Klf2/Klf4/Klf5* triple knockdown ESCs (Jiang et al., 2008) shared ~29% of differentially expressed genes (Figure 2D), thus suggesting that modulation of *Klf*s might be relevant for PiC specification.

Gene ontology analysis of the PiC expression profile denoted a consistent overrepresentation of genes in six Kyoto Encyclopedia of Genes and Genomes (KEGG) pathways, all related to cell shape and motility (Figure 2E). In keeping with the altered cytoskeleton architecture, 9% of L-Pro-regulated genes were structurally and/or functionally related to the cytoskeleton, whereas 12.8% were related to cell adhesion, cell junction, or cell motility (Figure 2C; Table S1). In line with the idea that cell motility/invasion is associated with extracellular matrix (ECM) remodeling, ~11% of the L-Pro-regulated genes were extracellular proteins, including secreted proteases, as well as modulators of their proteolytic activity (Table S1). These significant sets of genes regulated by L-Pro likely define the molecular signature that is required to direct and sustain the acquisition of the PiC motile phenotype. The PiC expression profile was also enriched in genes associated with six cancer-related KEGG pathways (Figure 2E; Table S1), among which there are members of the Janus kinase/signal transducers and activator (JAK/STAT), phosphatidylinositol 3-kinase (PI3K), and mitogen-activated protein kinase (MAPK) pathways, as well as the transforming growth factor (TGF)-beta pathway (Table S1). Collectively, these findings support the possibility that L-Pro may promote the acquisition of features typical of invasive cancer cells.

PiCs Are Invasive and Metastatic Pluripotent Stem Cells

To directly test PiC invasiveness, we first evaluated the effect of L-Pro on cell invasion in transwell assays. PiCs, but not ESCs, were able to migrate through Matrigel-coated transwells. More relevantly, >65% of migrating PiCs efficiently invaded a three-dimensional-Matrigel plug (Figure 3A). Interestingly, the migratory and invasive properties of PiCs at 500 cells/cm^2 (PiCs^{500}) were strongly reduced compared to PiCs^{50} generated at clonal density, i.e., 50 cells/cm^2 ($\geq$70%; Figure S1B). This latter finding supports the key role of the seeding density in defining the motile PiC phenotype. Moreover, PiCs generated from the feeder-independent E14Tg2a ESCs showed a highly motile/invasive phenotype, thus ruling out the possibility of an ESC line-specific effect of L-Pro (Figure S3).

We then asked if the migratory and invasive phenotype of PiCs correlated with metastatic potential in vivo. To this end, enhanced GFP (EGFP)-labeled ESCs or PiCs were injected intravenously into immunodeficient mice. The metastatic B16-BL6 melanoma cells were used as a positive control. Mice were sacrificed 4 weeks after injection, and the histology of liver and lung tissues was examined for macroscopic abnormalities. Whereas the ESC-injected mice showed morphologically normal tissues with no evidence of tumor masses, large teratomas were clearly visible in the lungs of PiC-injected mice (Figure 3C). Moreover, teratomas were EGFP-positive confirming that they originated from the exogenous cells (Figure 3D). These data provide direct evidence that PiCs have acquired metastatic properties and indicate that L-Pro-induced stem cells acquire two of the most decisive pathological traits of the so-called "migrating cancer stem cells," i.e., stemness and invasiveness.

L-Pro Induces an Embryonic-Stem-Cell-to-Mesenchymal-like Transition

Our data are also consistent with the possibility that L-Pro-induced morphological and motility phenotypes contribute to the acquisition of cell plasticity, likewise canonical epithelial-to-mesenchymal transition (EMT) (Yang and Weinberg, 2008). Thus, we hypothesized that L-Pro might trigger an EMT-like process in ESCs, namely an esMT. EMT is characterized by the induction of mesenchymal markers, such as N-cadherin (*N-cad*), vimentin (*Vim*), and matrix metallopeptidase 2 (*Mmp2*), and the concurrent downregulation of E-cadherin (*E-cad*), a major component of cell adherens junctions (Kalluri, 2009; Thiery et al., 2009). *N-cad, Vim*, and *Mmp2* were all upregulated in L-Pro-treated ESCs (Figure 4A). The transcription factor brachyury (*T*) was also strongly induced (Figures 4A and 4D). Notably, the expression of *T* has recently been associated with EMT during metastasis (Fernando et al., 2010; Sarkar et al., 2012). *N-cad* transcripts were detected from day 2 onward during the esMT, whereas *T* transcripts were induced at day 3 (Figure 4B), in a timeframe that correlated with the onset of the motile phenotype (Figure 1D). At the protein level, both N-CAD and T accumulated later on (Figure 4C). E-CAD, instead, was expressed at comparable levels in ESCs and PiCs (Figures 4E and 4F). Accordingly, the expression of the *E-cad* transcriptional repressors, *Snail* and *Slug*, were not significantly altered (Figure 4E). Nevertheless, altered trafficking and cell surface distribution of the E-CAD protein can also contribute to its functional downregulation (Cavallaro and Christofori, 2004). In line with this notion, we observed a reduction of E-CAD protein at cell-cell junctions, accompanied by an accumulation of E-CAD in perinuclear vesicular-like compartments from day 3 of the esMT (Figures 4G and 4H).

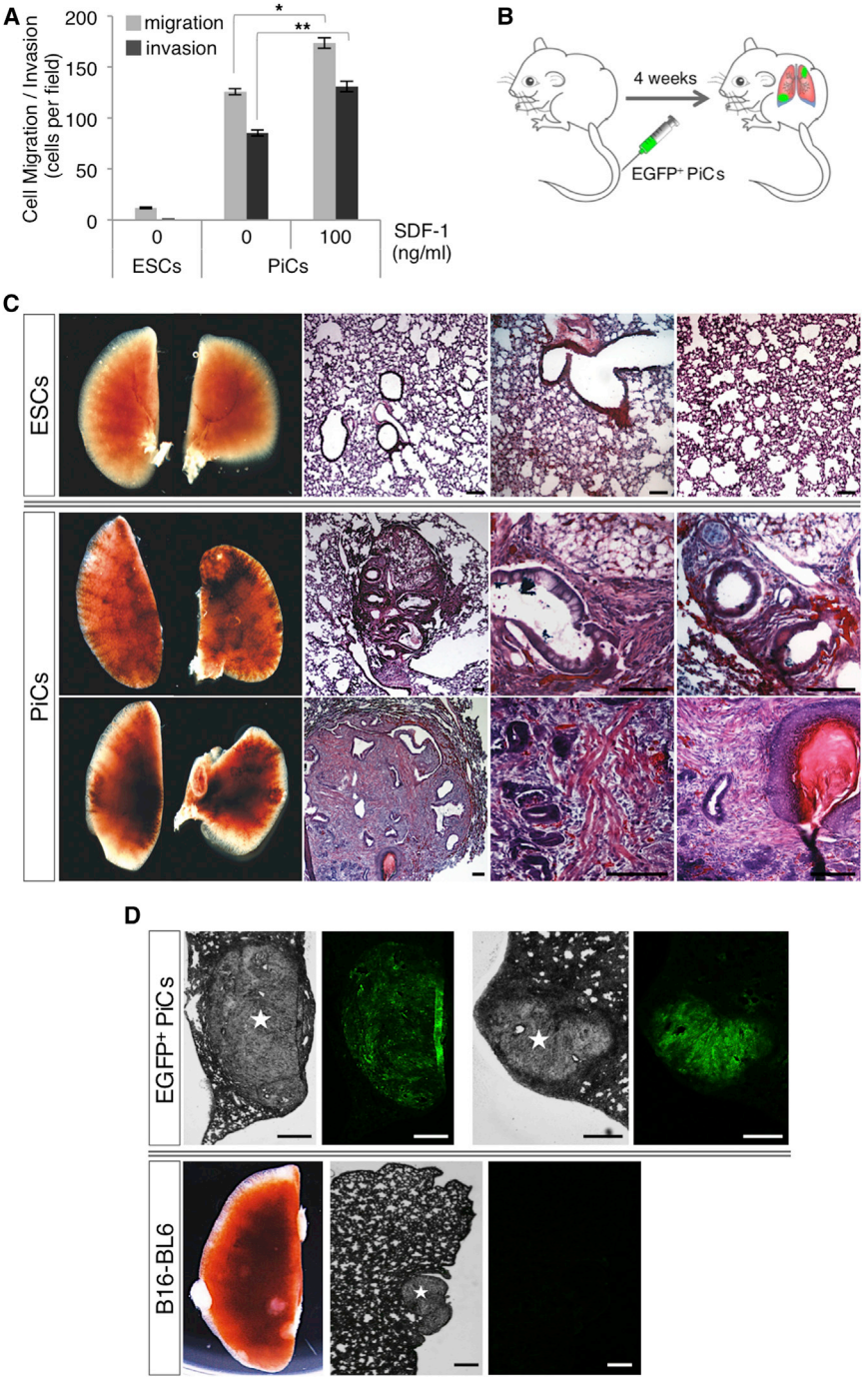

Figure 3. Invasive and Metastatic Potential of L-Pro-Treated ESCs

(A) Parallel migration (gray bars) and cell invasion (black bars) transwell assays measuring migration/invasion of ESCs and PiCs toward a FBS gradient (1%–15%) ± SDF-1 (100 ng/ml). The average number of migrating and invading PiCs is indicated. Data are mean ± SD; n = 3; *p < 0.05; **p < 0.001.

(B) Schematic representation of in vivo metastasis assay. Nonobese diabetic (NOD)/SCID mice were injected intravenously with either EGFP-marked ESCs, PiCs (1×10^6 cells), or B16-BL6 melanoma cells (2×10^5).

(C) Lungs (left panels) and hematoxylin and eosin-stained lung tissue sections (right panels) from ESC/PiC-injected mice, showing large teratomas in two PiC-injected mice; n = 5/group.

(D) Representative photomicrographs of lung tissue sections showing $EGFP^+$ PiC-derived teratomas (white stars, upper panel) or a B16-BL6 melanoma cell-derived tumor used as a control (white star, lower panel).

Scale bars represent 100 μm (C) and 500 μm (D). See also Figure S3.

To assess if L-Pro-induced esMT might impact on the differentiation potential, we compared both the cardiac and neuronal differentiation kinetics of PiCs and ESCs. Despite the fact that PiCs, but not ESCs, expressed high levels of the panmesodermal marker *brachyury*, the kinetics of cardiac markers expression were comparable in the two lines (Figure S4A). On the other hand, whereas neuronal and glia markers displayed similar levels in PiCs and ESCs, their kinetic of expression was delayed in PiCs (Figure S4B). These data suggest that L-Pro-induced esMT does not promote or anticipate cardiac differentiation, whereas it slightly delays neural differentiation. Finally, to identify critical factors involved in the L-Pro-induced esMT, we focused our attention on the protein kinase domain-containing, cytoplasmic

(PKDCC) kinase. *Pkdcc* was the most highly upregulated protein kinase-coding gene in L-Pro-treated ESCs and was induced from day 2 onward (Figure 4I; Table S1). *Pkdcc* is required for the round-to-flat shape transition of chondrocytes occurring during bone development (Imuta et al., 2009) and is involved in the control of protein export from the Golgi (Kinoshita et al., 2009). Of note, E-CAD accumulated in the Golgi complex in PiCs (Figure 4H). Interestingly, we observed that transient *Pkdcc*-silencing inhibited the acquisition of the flat morphology in L-Pro-treated cells (Figure 4J). Thus, L-Pro is sufficient to promote the esMT that is dependent, at least in part, on *Pkdcc*.

L-Pro Alters the Epigenetic Signature of ESCs

To gain clues as to the mechanism through which the simple exposure to a nonessential amino acid induces dramatic changes in gene transcription and ESC behavior, we hypothesized that L-Pro might act as an epigenetic modifier. Consistent with this idea, the silencing of *Jmjd1a,* a H3K9 demethylase, forces ESCs toward a PiC-like phenotype, i.e., flat morphology, sensitivity to trypsin digestion and upregulation of *Fgf5* and *T* (Loh et al., 2007). We therefore tested whether L-Pro is sufficient to alter methylation levels of various critical histone lysine residues in ESCs. L-Pro augmented the global levels of H3K9me2 and H3K9me3, as well as the levels of H3K36me3 (Figure 5A, left panel). In contrast, the levels of H3K4me3 and H3K27me3 were unaltered (Figure 5A, right panel). More relevantly, L-Pro triggered a genome-wide reprogramming of H3K9 and H3K36 methylation status. H3K9 methylation was significantly altered at 16,621 sites, with the highest increase in methylation occurring at noncoding intergenic regions of the genome (Figures 5B, S5A, and S5B). Genes showing PiCs-enriched H3K9me3 occupancy at proximal and distal regulatory regions are reported in Figure S5C. H3K9 methylation status changed in a significant fraction (27%) of the 1,521 L-Pro-deregulated genes ($p < 0.05$; Figure 5C, upper panel). Moreover, those genes displaying a modified H3K9 methylation status were enriched in pathways relevant for the esMT process (Figure 5C, lower panel). Consistently, genes downregulated in PiCs displayed an increase in H3K9me3 at regulatory regions (Figure 5D). Noteworthy, repetitive elements were frequently detected at sites displaying increased H3K9me3, suggesting an induced local heterochromatin spreading into nearby genes that influences their expression (Figure 5D). Remarkably, chromatin immunoprecipitation sequencing (ChIP-seq) showed the highest H3K9me3 enrichment at constitutive heterochromatin, i.e., pericentromeres and gene deserts, indicating that L-Pro induces heterochromatin reorganization toward more dense structures in the nucleus (Figures S5B and S5D).

Differentially expressed genes that were not altered in the H3K9me3 profile might be regulated by additional epigenetic marks. Consistently, ChIP-PCR analysis revealed a significant enrichment of the H3K27me3-repressive mark at promoters of L-Pro-downregulated genes (Figure S5E). Conversely, L-Pro-upregulated genes showed reduced levels of H3K27me3 and increased levels of the H3K4me3-permissive mark. Consistent with a global H3K9 methylation gain, we detected an overall increase of H3K9 methylation at both promoter and gene body regions (Figure S5E).

We also investigated the whole-genome profile of H3K36me3 and observed 8,648 significant peaks altered by L-Pro treatment (Figure 5E). Intragenic regions of differentially methylated clusters of loci were H3K36me3-increased in PiCs relative to ESCs (Figure S5F), and a significant fraction (41%; $p < 0.05$) of PiC-specific genes showed significant H3K36me3 changes according to the transcriptional status (Figures 5F and 5G). Notably, L-Pro induced H3K36me3 enrichment at noncoding regions, in line with recent evidence that H3K36me3 might promote heterochromatin formation (Figure S5G; Chantalat et al., 2011). Collectively, our findings support a role of L-Pro as a genome-wide inducer of H3K9 and H3K36 methylation in pluripotent stem cells.

Vitamin C Reverts the PiC Phenotype and Induces H3K9 and H3K36 Demethylation

Increasing evidence indicates that demethylation of H3K36 and H3K9 is required for an efficient somatic/pre-induced pluripotent stem cell (iPSC) to iPSC transition (Chen et al., 2013; Wang et al., 2011). This crucial step in cell reprogramming is controlled by vitamin C, which is a cofactor of H3K9 jumonji demethylases (Wang et al., 2011) and a key regulator of stem cell differentiation and somatic cell reprogramming (Cao et al., 2012; Esteban et al., 2010; Yang et al., 2008). We thus tested the effect of vitamin C on the PiC phenotype. Remarkably, vitamin C almost completely reverted the esMT at the morphological level, promoting a mesenchymal-like-to-embryonic-stem-cell transition (MesT), even in the presence of L-Pro. Remarkably, vitamin C mimicked the phenotype caused by L-Pro removal (Figure 6A). To rule out the possibility that vitamin C induced selection of ESCs rather than PiC-to-ESC reversion, freshly generated PiCs (P_0) were directly plated at low density and the frequency of domed and flat colonies was assessed in the different culture conditions. When PiCs were plated in the presence of L-Pro, about 10% of the colonies showed a domed phenotype (ESCs; Figures S6A and S6B), which corresponds to the degree of heterogeneity observed in freshly generated PiCs. Indeed, PiCs culture consistently display 10%–15% of domed (ESCs) and 85%–90% of flat (PiCs) colonies (Casalino et al., 2011). Remarkably, when PiCs were plated either in the absence of L-Pro or in the presence of L-Pro plus vitamin C (Figures S6A and S6B), the percentage of domed colonies (ESCs) increased up to 50%. Importantly,

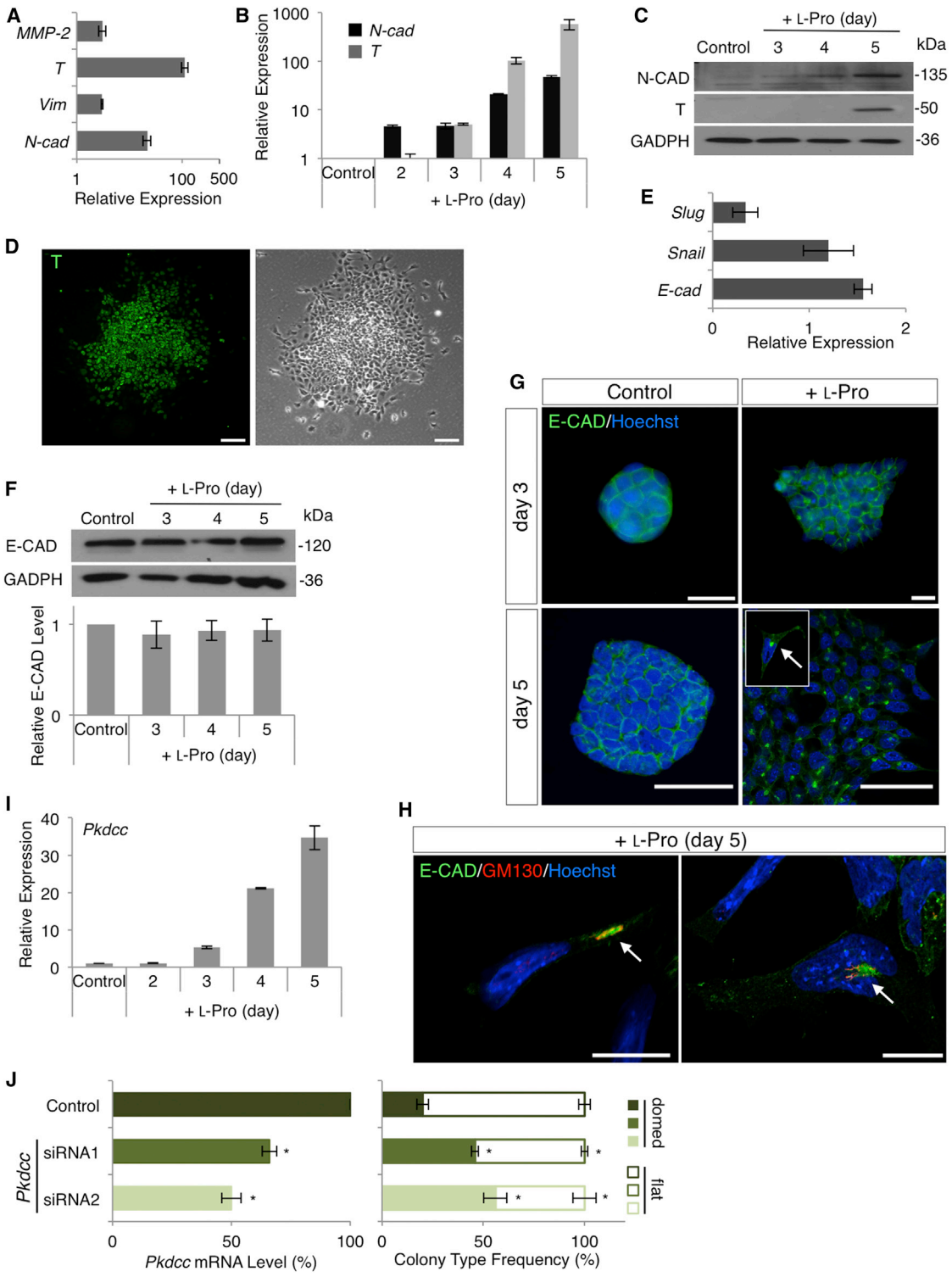

Figure 4. L-Pro Induces an esMT

(A) qPCR analysis of the expression of EMT markers in L-Pro-treated versus untreated ESCs (day 5).

(B and C) Time course of *N-cad* and *T* expression measured by qPCR (B) and western blot (C) analysis. GAPDH, glyceraldehyde 3-phosphate dehydrogenase.

(D) Microphotographs of *T* immunostaining (left panel) and phase contrast (right panel) of PiCs. The scale bar represents 100 μm.

(legend continued on next page)

the total number of colonies generated in the different culture conditions was comparable. Moreover, the migratory and invasive properties of the vitamin C-treated PiCs ($ESCs^{Rev}$) resembled the one of ESCs (Figure 6B). Finally, both the frequency and the timing of appearance of flat colonies were comparable in L-Pro-treated ESCs and $ESCs^{Rev}$ (Figures 6C and 6D), thus ruling out the possibility that $ESCs^{Rev}$ were primed for PiC formation. All together these findings provide evidence that vitamin C reverts both the morphological and the functional phenotype of PiCs toward that of ESCs. At the molecular level, vitamin C repressed L-Pro-induced *T* expression and reverted L-Pro-induced downregulation of *Inhbb* expression (Figure 6E). Furthermore, vitamin C inhibited the L-Pro-induced increase in H3K9me3 and H3K36me3 levels to an extent that was comparable to that observed following L-Pro withdrawal. Thus, vitamin C induces the MesT by remodeling the epigenetic signature of PiCs (Figure 6F). To get insight into the epigenetic mechanism underlying vitamin C-induced reversion of the PiC phenotype, we knocked down *Jmjd1a*. To this end, PiCs were transfected with either shRNA constructs targeting different regions of the transcript *(Jmjd1a-* shRNA1 and shRNA2) or control shRNAs *(Jmjd1a- shRNA1mut* and *Luciferase* shRNA), as previously described (Loh et al., 2007). Of note, neither the morphology nor the expression of pluripotency markers was altered in *Jmjd1a KD* (≥70% gene silencing; Figure S6D) compared to controls PiCs (data not shown). We thus plated *Jmjd1a KD* and control PiCs in the presence or the absence of vitamin C and analyzed the frequency of flat and domed colonies. The frequency of appearance of domed colonies was nearly identical in vitamin C-treated *Jmjd1a KD* and control PiCs (Figure S6E). Notably, the effect of vitamin C mimicked the one achieved by L-Pro removal (Figure S6E). These data indicate that downregulation of *Jmjd1a* is not sufficient to prevent vitamin-C-dependent PiC-to-ESC reversion. Remarkably, neither glutathione nor *N*-acetyl-L-cysteine were able to revert PiCs toward an ESC phenotype (Figure S6C), thus excluding the possibility that vitamin C acts in this process through its antioxidant activity.

DISCUSSION

How metabolites regulate stem cell biology represents a major challenge and is still poorly understood. Here, we uncover an unexpected role of L-Pro as a key regulator of mouse ESC migratory and invasive phenotype, revealing that L-Pro is a potent epigenetic modifier. L-Pro, and in particular its mitochondrial catabolism, has become an important area of study being at the crossroads of key metabolic pathways, including citric acid cycle, polyamines biosynthesis, and urea cycle (Phang et al., 2012). Despite that L-Pro is a nonessential amino acid (Phang et al., 2008), we demonstrate that the addition of L-Pro in ESC culture medium is sufficient to induce a previously unforeseen esMT, which converts compacted/clustered ESCs into scattered, freely motile pluripotent stem cells. Of note, this phenotype was not observed in previous studies (Casalino et al., 2011; Washington et al., 2010), most likely because it markedly increased when ESCs are seeded at clonal density in the presence of L-Pro. Accordingly, PiCs generated at higher density ($PiCs^{500}$) showed poor migratory and invasive properties compared to PiCs generated at clonal density ($PiCs^{50}$) indicating that seeding density strongly influences the EMT-like phenotype of PiCs.

The L-Pro-induced esMT is accompanied by a global remodeling of the ESC transcriptome, which nicely correlates with the phenotypic variation observed. Indeed, genes involved in the control of cell cytoarchitecture, adhesion, and migration/invasiveness are largely affected by L-Pro. Notably, despite this extensive remodeling of the transcriptome, expression levels of the pluripotency-associated factors (*Oct4*, *Nanog*, and *Sox2*) and the developmental pluripotency-associated gene *Dppa3* (*Stella*) are comparable in PiCs and ESCs. Furthermore, PiCs, like ESCs, are REX1 (Zfp42)-positive (≥95%) and show similar in vitro differentiation kinetics. This molecular signature and the fact that PiCs strictly depend on LIF for self-renewal (Casalino et al., 2011) suggest that they define a population of inner cell mass-like cells that have acquired a motile and invasive phenotype.

(E) qPCR analysis of *E-cad*, *Snail*, and *Slug* expression in L-Pro-treated versus untreated ESCs (day 5).
(F) Time course of E-CAD expression in L-Pro-treated ESCs by western blot analysis. Densitometric analysis of E-CAD protein levels relative to untreated ESCs after normalization to GAPDH.
(G) Images of E-CAD immunostaining of control and L-Pro-treated ESCs using conventional (upper panels) or confocal (lower panels) fluorescence microscopy. White arrow (inset) indicates the vesicular perinuclear localization of E-CAD. The scale bar represents 50 μm.
(H) Fluorescence confocal photomicrographs showing colocalization (white arrows) of E-CAD with the Golgi marker GM130. Nuclei were counterstained with Hoechst. The scale bar represents 20 μm.
(I) Time course of *Pkdcc* expression in L-Pro-treated ESCs by qPCR. (A, B, E, and I). Data are fold change compared to control ESCs after normalization to *Gapdh*.
(J) Downregulation of *Pkdcc* expression by siRNAs (left panel) in L-Pro-treated ESCs (day 5). Data are fold change in gene expression compared to control (nontargeting siRNA). Effect of *Pkdcc*-silencing on the colony-type frequency (right panel); data are mean ± SD, ~100 colonies scored; n = 3; *p < 0.01.
See also Figure S4.

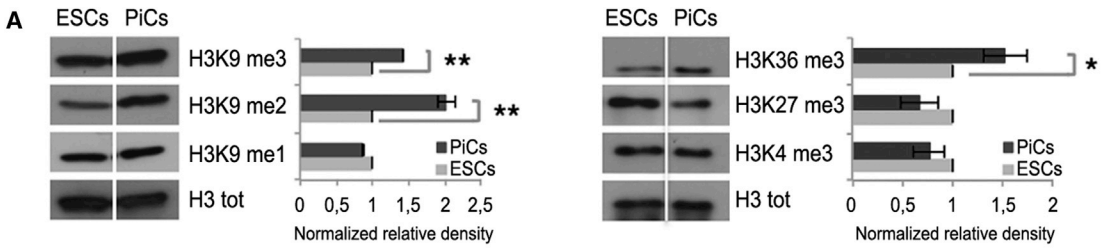

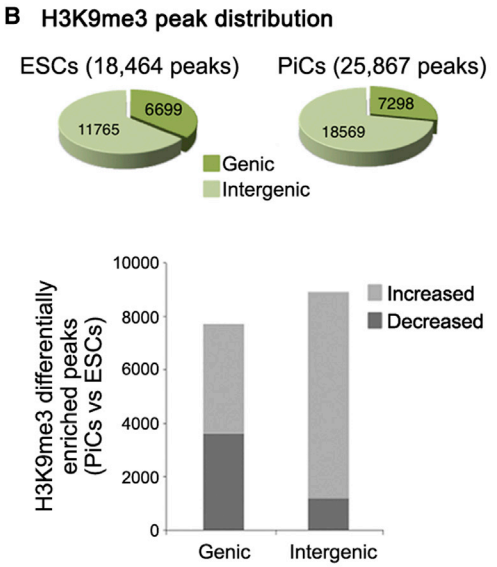

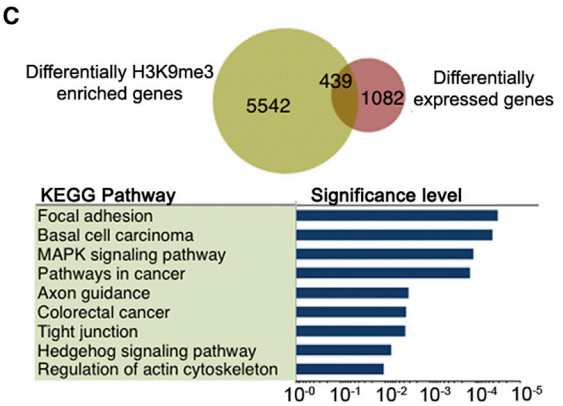

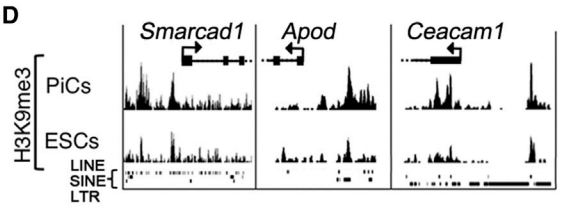

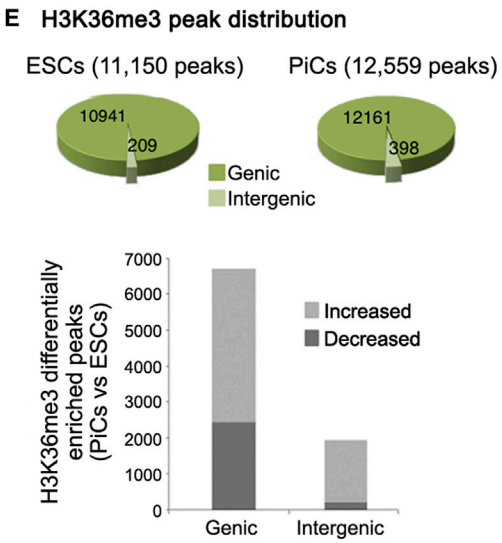

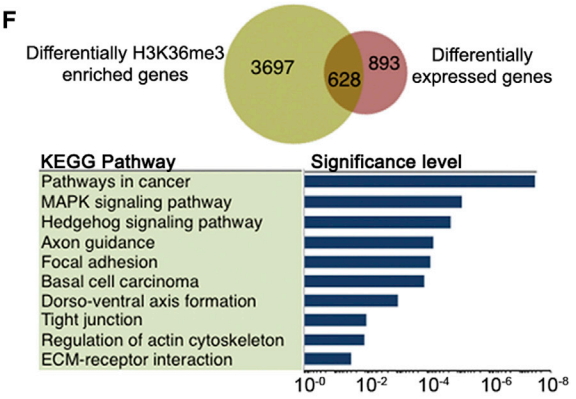

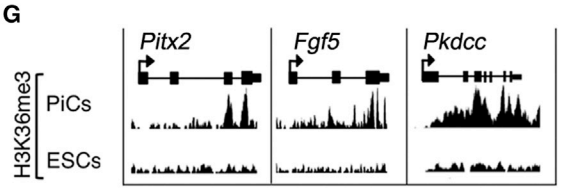

(legend on next page)

Interestingly, L-Pro-induced esMT is accompanied by a significant increase in H3K9 and H3K36 methylation levels as well as by a global remodeling of the H3K9me3 and H3K36me3 marks. This L-Pro-induced esMT is fully reversible either after L-Pro withdrawal or by addition of ascorbic acid (vitamin C), promoting a MesT and inducing the reduction of H3K9 and H3K36 methylation levels.

To the best of our knowledge, only three metabolites, L-threonine, butyrate, and vitamin C, have been identified so far that act as epigenetic modulators of ESC self-renewal and/or somatic cell reprogramming (Mali et al., 2010; Shyh-Chang et al., 2013; Wang et al., 2009). Interestingly, L-threonine, which is the only amino acid among these metabolites, influences H3K4me3 by controlling the abundance of S-adenosylmethionine, leaving other lysine residues unaltered (Shyh-Chang et al., 2013). This intriguing specificity is also exerted by L-Pro that conversely influences the global level of trimethylation of lysines K9 and K36, which would likely exert a wider effect on gene expression. This is consistent with the extensive molecular and phenotypic variations induced by L-Pro on ESCs, as, for instance, the striking acquisition of motility and invasiveness. Most remarkably, L-Pro-induced global increase of H3K9 and H3K36 trimethylation preferentially occurs at noncoding intergenic regions and constitutive heterochromatin. Whereas H3K9me3 is a well-known repressive heterochromatic mark, the H3K36me3 deposition within heterochromatin domains has only recently emerged. H3K36me3 might thus contribute to the establishment of a transcriptionally unfavorable chromatin conformation by recruiting repressive complexes (Chantalat et al., 2011). Our data suggest that L-Pro can induce heterochromatization, increasing H3K9me3 and H3K36me3 especially at pericentromeric and gene desert regions, and imply that there is a hierarchy of target chromatin regions and associated noncoding elements that are more sensitive to the effect of L-Pro in ESCs.

Thus, our findings add to the emerging evidence that metabolites are key mediators of epigenetic regulation of stem cell fate and strengthen the role of the amino acids in this process. Yet how metabolites control chromatin modifiers in space and time, translating a dynamic metabolic state into a histone code, is still a key unresolved question (Folmes et al., 2012; Phang et al., 2013; Sassone-Corsi, 2013; Zhang et al., 2012). Interestingly, it has been recently proposed that the concentration of metabolites and their biosynthetic enzymes may localize to chromatin subdomains promoting the clustering of relevant DNA and histone modifications at specific genomic loci (Katada et al., 2012). It is thus tempting to speculate that specific histone-modifying enzymes might sense the presence of L-Pro and eventually translate this signal into different histone maps. Interestingly, we have shown that vitamin C, which is a cofactor of the Jumonji-family histone demethylases, antagonizes the effect of L-Pro on H3K9me3 and H3K36me3 levels. Of note, knockdown of *Jmjd1a* (H3K9 demethylase) does not prevent vitamin C-induced PiC-to-ESC reversion. However, because many other vitamin C-regulated histone modifier enzymes might be involved in this process, further studies are needed to reveal its molecular nature.

We believe that our findings have several implications for stem cell biology. First, it has been shown that the reprogramming process initiates through a mesenchymal-to-epithelial transition (MET) (Li et al., 2010; Samavarchi-Tehrani et al., 2010) and that vitamin C-dependent decrease of H3K9/H3K36 methylation levels promote somatic/pre-iPSC to iPSC transition (Chen et al., 2013; Wang et al., 2011). Thus L-Pro and vitamin C exert opposite effects on H3K9 and H3K36 methylation status, regulating antagonistic cellular processes relevant for cell reprogramming. Recently, it was reported that vitamin C also promotes Tet-mediated DNA demethylation (Blaschke et al., 2013). It will be thus interesting to investigate the effect of L-Pro on DNA methylation.

Second, the L-Pro/vitamin C-regulated esMT-MesT switch is reminiscent of the transient EMT-MET switch that has been proposed as a driving force of metastasis,

Figure 5. L-Pro Modifies the Epigenomic Signature of ESCs

(A) Western blot analysis of global H3K9 mono-, di-, and trimethylation (left) and H3K4, K27, and K36 trimethylation (right) levels in PiCs compared to ESCs. Densitometric analysis is relative to control ESCs after normalization to total histone H3. Data are mean ± SD (n = 3); *p < 0.05; **p < 0.001.

(B) Genome-wide H3K9me3 peaks (upper panel) and SICER-based differential distribution (lower panel) of H3K9me3 binding sites at genic and intergenic regions in PiCs versus ESCs.

(C) Venn diagram correlating microarray gene expression and ChIP-seq data (p = 0.03; Fisher's exact test; upper panel). KEGG pathway enrichment analysis of 439 loci that are H3K9me3 differentially enriched and deregulated (lower panel).

(D) Snapshot of H3K9me3 profile at *Smarcad1*, *Apod*, and *Ceacam1* genes.

(E) Genome-wide H3K36me3 peaks (upper panel) and SICER-based distribution (lower panel) of differential H3K36me3 binding sites at genic and intergenic regions in PiCs versus ESCs.

(F) Venn diagram correlating microarray gene expression and ChIP-seq data (p = 0.03; Fisher's exact test; upper panel) and KEGG pathways enrichment analysis of 628 loci that are H3K36me3 differentially enriched and deregulated (lower panel).

(G) Snapshot of H3K36me3 profile at *Pitx2*, *Fgf5*, and *Pkdcc* genes.

See also Figure S5 and Table S2.

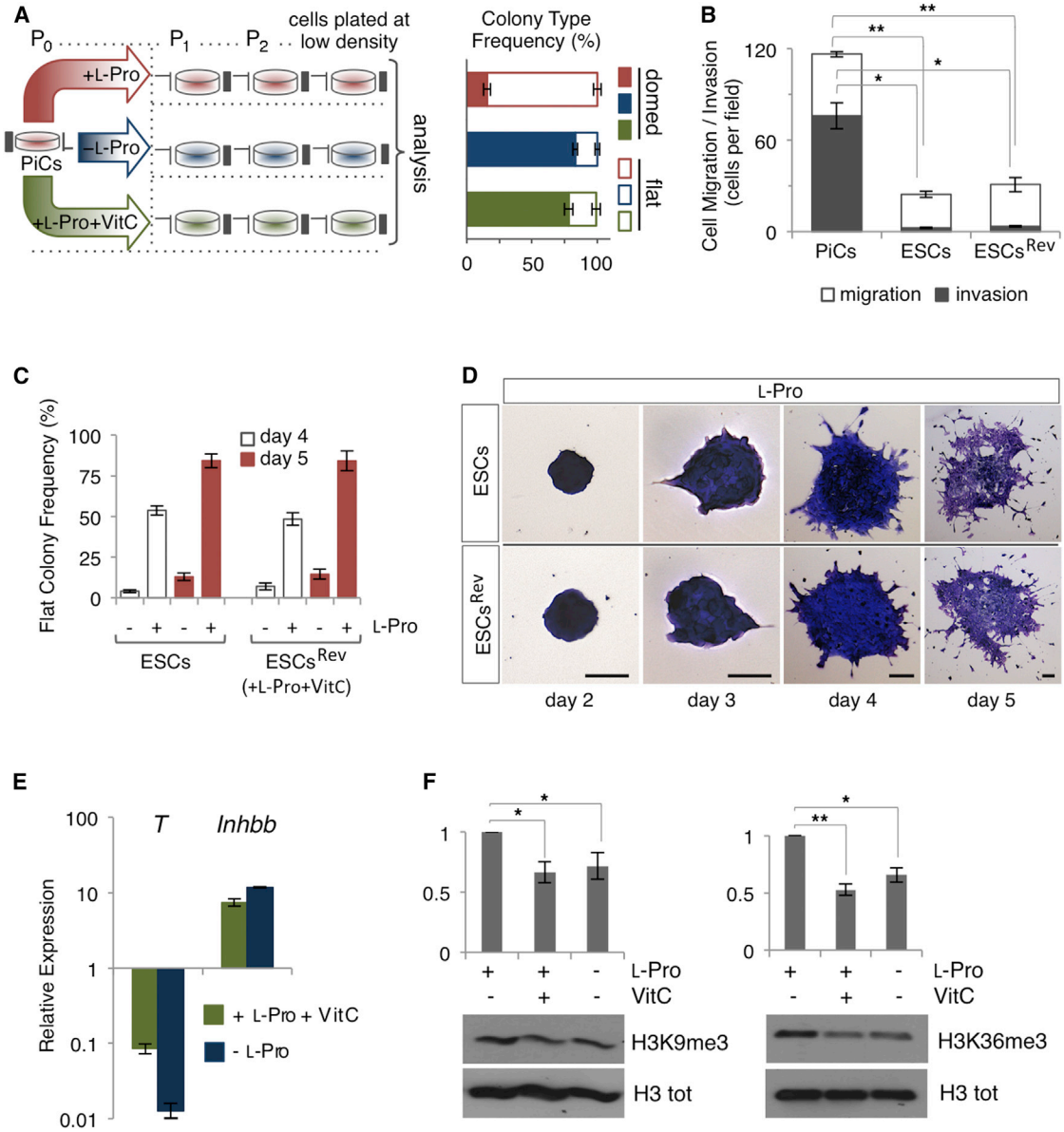

Figure 6. Vitamin C Reverts the PiC Phenotype Inducing H3K9 and H3K36 Demethylation

(A) Schematic representation of the experimental strategy. Freshly generated PiCs (P_0) were passaged twice (P_1 and P_2) with L-Pro (control), without L-Pro, or with L-Pro + VitC. Cells were then plated at 500 cells/cm^2, grown for 5 days, and processed for colony phenotype assay (domed versus flat; right panel). Data represent the percentage of colony-type frequency and are mean ± SD; ~100 colonies scored; n = 3.

(B) Migration (white bars) and cell invasion (gray bars) transwell assays of ESCs, PiCs, and vitamin C-treated PiCs (ESCs^{Rev}) toward a FBS gradient (1%–15%). The average number of migrating and invading cells is indicated. Data are mean ± SD; n = 3; *$p < 0.01$; **$p < 0.0001$.

(C and D) Comparative analysis of L-Pro-induced phenotypic transition in ESCs^{Rev} and ESCs. (C) Flat colony frequency of control (untreated) and L-Pro-treated ESCs and ESCs^{Rev} at days 4 and 5 after plating. Data are mean ± SD (n = 3; ~100 colonies were scored in each experiment). (D) Time course analysis of PiC formation in L-Pro-treated ESCs versus ESCs^{Rev}. Representative photomicrographs of crystal violet-stained, L-Pro-treated ESCs and ESCs^{Rev} colonies at the indicated time points. The scale bars represent 50 μm.

(E) qPCR analysis of *T* and *Inhbb* expression. Data are fold change in gene expression compared to control (+L-Pro) after normalization to *Gapdh*.

(F) Western blot analysis of H3K9me3 and H3K36me3 levels (lower panels). Densitometric analysis (upper panels) is relative to control ESCs after normalization to total histone H3. Data are mean ± SD (n = 2); *$p < 0.05$; **$p < 0.01$.

See also Figure S6.

largely influenced by microenvironment (Brabletz et al., 2005). Indeed, it is proposed that induction of EMT confers migrating properties to cancer stem cell (Brabletz, 2012). How this occurs is still poorly defined. Interestingly, the ECM is mostly composed of collagen (80%) and is considered as a reservoir of mobilizable L-Pro (Phang et al., 2008). Here, we suggest that L-Pro, which is released from ECM degradation during tumor invasion, may act as environmental cue of the EMT to control tumor dissemination. Moreover, L-Pro metabolism is dysregulated in cancer (Liu et al., 2012; Phang et al., 2012) and L-Pro synthesis is associated with tumor progression and aggressiveness (Scott et al., 2011), yet the mechanisms remain largely unsolved. Although much work remains to be carried out to assess the in vivo relevance of L-Pro as signal molecule, our findings contribute to elucidating its role in regulating stem cell behavior and provide insights into the mechanisms by which metabolites control stem cell fate.

EXPERIMENTAL PROCEDURES

Cell Cultures

Wild-type TBV2 (129/SvP), β-actin/EGFP TBV2 and E14Tg2a (E14) mouse ESCs were cultured as described (Casalino et al., 2011). PiCs were generated as previously described (Casalino et al., 2011). Briefly, ESCs were seeded at low density (50–500 cells/cm^2) and grown in the presence of L-Pro (50–500 μM) for 5 days. Freshly generated PiCs (P_0) consistently displayed 10%–15% of domed (ESCs) and 85%–90% of flat (PiCs) colonies. ESC treatment details are reported in the Supplemental Experimental Procedures. B16-BL6 melanoma cells were cultured in RPMI, 10% FBS, 2 mM glutamine, and 100 U/ml penicillin/streptomycin.

In Vitro Differentiation

For cardiomyocyte differentiation, ESCs/PiCs were allowed to differentiate through embryoid bodies in hanging drop (500 cells/drop) as described (Parisi et al., 2003). Neuronal differentiation was performed as described (Fico et al., 2008).

Pkdcc Silencing

ESCs were plated at 50 cells/cm^2 in the presence of L-Pro (150 μM) and transfected twice, at 30 and 54 hr after plating, with *Pkdcc* siRNAs or control (150 nM; Silencer Select siRNA; Ambion) using Lipofectamine RNAiMAX (Invitrogen). tBLOCK-iT Alexa Fluor Red (50 nM; Ambion) was used to assess the transfection efficiency.

Jmjd1a Silencing

PiCs were transfected with 2 μg of DNA plasmids (Loh et al., 2007) using Lipofectamine 2000 (Invitrogen). Puromycin (1 μg/ml; Sigma) selection started 1 day after transfection and was maintained for 3 days. Puromycin-resistant cell pools were either harvested for RNA extraction or plated at low density without L-Pro or with L-Pro ± vitamin C (VitC) (500 μM) and the resulting colonies analyzed at day 5 after plating.

RNA Preparation and Quantitative RT-PCR

Total RNAs were isolated using RNeasy mini kit and analyzed at the Ohio State University microarray facility. QuantiTect Reverse Transcription kit (QIAGEN) and SYBR Green PCR master mix (FluoCycle II SYBR; EuroClone) were used for quantitative PCR (qPCR) analysis. Primers are in the Supplemental Experimental Procedures.

Cell Migration/Invasion and Metastasis Assays

Migration assays were performed using polycarbonate (5 μm pore; Costar) or polyester membrane transwells (8 μm pore; BD Biosciences). ESCs were plated at 50 or 500 cells/cm^2 in complete medium ± L-Pro. At day 5, cells were detached with Accutase (Sigma) and 2 × 10^4 ESCs/PiCs were incubated for 20–22 hr. EGF, insulin, SDF-1 (Sigma-Aldrich), and Cyr61 (R&D Systems) were added in 1% FBS. Invasion assays were performed using BD BioCoat Growth Factor Reduced MATRIGEL Invasion Chambers (Supplemental Experimental Procedures).

EGFP-marked ESCs were plated at 50 cells/cm^2 and grown in complete medium ± L-Pro for 5 days. ESCs/PiCs (1 × 10^6 cells) and B16-BL6 (2 × 10^5) were injected into the tail veins of 7-/8-week-old severe combined immunodeficiency (SCID) mice (five mice/group; Charles River Laboratories). ESCs/PiCs were also injected subcutaneously as control. After 4 weeks, mice were sacrificed and paraformaldehyde-perfused tissues were explanted and photographed (Leica MZ16 FA stereomicroscope) before embedding in optimal cutting temperature. The care and husbandry of mice and metastasis experimental procedures were in accordance with European Directives No. 86/609 and with Italian D.L. 116 and approved by the Institute of Genetics and Biophysics (IGB) veterinarian.

Time-Lapse Experiments

ESCs were seeded on gelatin-coated plates at 50 cells/cm^2 and grown in complete medium ± L-Pro (150 μM). Images were captured (20×) every 5 min for about 24 hr using Nikon Eclipse TE2000-E inverted microscope.

Immunofluorescence Analysis

Cells were fixed (4% paraformaldehyde) and permeabilized (0.1% Triton X-100) at room temperature. After incubation with the primary antibodies (Supplemental Experimental Procedures), cells were incubated with the appropriate secondary antibodies (Alexa Fluor 1:200; Molecular Probes). Phalloidin-TRITC (1:300; Sigma) was used for actin staining. For REX1 immunofluorescence, 1–1.5 × 10^4 ESCs/PiCs were centrifuged at 900 rpm for 15 min (Cytocentrifuge; Thermo Scientific). Cytospin samples were processed as above. Images were taken using inverted (DMI6000B; Leica Microsystems) and confocal (TCS-SP2-AOBS; Leica Microsystems) microscopes. Leica FW4000 and AF6000 software were used for image acquisition/elaboration.

Western Blot Analysis

Cell lysates were prepared with ice-cold radio immunoprecipitation assay (RIPA) lysis buffer. Cell pellets were resuspended in Triton buffer for histone extraction. Primary antibodies are reported in the Supplemental Experimental Procedures. Detection

was performed with enhanced chemiluminescence reagents (Amersham Biosciences). Densitometric analysis was carried out using the software GelEval 1.35.

ChIP-qPCR and -Sequencing

Chromatin immunoprecipitation was performed as previously described (De Bonis et al., 2006). Suitable amount of chromatin was incubated with 5–10 μg of the indicated antibodies (Supplemental Experimental Procedures). Immunoprecipitated complexes were recovered with protein A sepharose (Pharmacia), washed with low and high salt buffers, reverse-crosslinked, and purified. Primers are reported in the Supplemental Experimental Procedures. The statistical significance of the qPCR results was assessed using the Student's t test.

H3K9me3 and H3K36me3 immunoprecipitated samples were prepared for SOLiD System 4.0 (Applied Biosystems)-based sequencing. Mapping to the mouse reference genome and peak-finding software are reported in the Supplemental Experimental Procedures.

ACCESSION NUMBERS

The Gene Expression Omnibus accession numbers for microarray and ChIP-seq data are GSE50603 and GSE50477, respectively.

SUPPLEMENTAL INFORMATION

Supplemental Information includes Supplemental Experimental Procedures, six figures, two tables, and three movies and can be found with this article online at http://dx.doi.org/10.1016/j.stemcr.2013.09.001.

ACKNOWLEDGMENTS

We are grateful to Rosalind Gunby and Monica Autiero for careful reading and critical comments of the manuscript. We thank the Animal House and the Integrated Microscopy Facilities of IGB-Consiglio Nazionale delle Ricerche (CNR) and the Bioinformatic Core Facility of Tigem. Laura Casalino is acknowledged for providing reagents and Gennaro Andolfi, Vincenzo Mercadante (Next Generation Sequencing Core Facility), and Gabriele Di Napoli for technical assistance. We thank Dr. Huck Hui NG for kindly providing *Jmjd1a* shRNA constructs. We are grateful to Francesco Gagliardi, Cecilia Fernandez, and Annamaria Carissimo for bioinformatic support. This work is supported by Associazione Italiana per la Ricerca sul Cancro grants 11599 (to G.M.) and 4497 (to G.S.), European Community's Seventh Framework Programme ENDOSTEM n. 241440 (to G.M.), Epigenomics Flagship Project (EPIGEN) MIUR-CNR (to G.M., M.R.M., and C.A.), and Italian Ministry of Education-University-Research (MIUR-PRIN) (to G.M. and G.S.). E.J.P. is supported by a grant from Medical Research in Italy (RBNE08HM7T-003). G.S is supported by grants from European Research Council (268836) and CARIPLO Foundation.

Received: March 1, 2013
Revised: September 11, 2013
Accepted: September 12, 2013
Published: October 10, 2013

REFERENCES

Blaschke, K., Ebata, K.T., Karimi, M.M., Zepeda-Martínez, J.A., Goyal, P., Mahapatra, S., Tam, A., Laird, D.J., Hirst, M., Rao, A., et al. (2013). Vitamin C induces Tet-dependent DNA demethylation and a blastocyst-like state in ES cells. Nature *500*, 222–226.

Brabletz, T. (2012). EMT and MET in metastasis: where are the cancer stem cells? Cancer Cell *22*, 699–701.

Brabletz, T., Jung, A., Spaderna, S., Hlubek, F., and Kirchner, T. (2005). Opinion: migrating cancer stem cells - an integrated concept of malignant tumour progression. Nat. Rev. Cancer *5*, 744–749.

Brons, I.G., Smithers, L.E., Trotter, M.W., Rugg-Gunn, P., Sun, B., Chuva de Sousa Lopes, S.M., Howlett, S.K., Clarkson, A., Ahrlund-Richter, L., Pedersen, R.A., and Vallier, L. (2007). Derivation of pluripotent epiblast stem cells from mammalian embryos. Nature *448*, 191–195.

Cao, N., Liu, Z., Chen, Z., Wang, J., Chen, T., Zhao, X., Ma, Y., Qin, L., Kang, J., Wei, B., et al. (2012). Ascorbic acid enhances the cardiac differentiation of induced pluripotent stem cells through promoting the proliferation of cardiac progenitor cells. Cell Res. *22*, 219–236.

Casalino, L., Comes, S., Lambazzi, G., De Stefano, B., Filosa, S., De Falco, S., De Cesare, D., Minchiotti, G., and Patriarca, E.J. (2011). Control of embryonic stem cell metastability by L-proline catabolism. J. Mol. Cell Biol. *3*, 108–122.

Cavallaro, U., and Christofori, G. (2004). Cell adhesion and signalling by cadherins and Ig-CAMs in cancer. Nat. Rev. Cancer *4*, 118–132.

Chantalat, S., Depaux, A., Héry, P., Barral, S., Thuret, J.Y., Dimitrov, S., and Gérard, M. (2011). Histone H3 trimethylation at lysine 36 is associated with constitutive and facultative heterochromatin. Genome Res. *21*, 1426–1437.

Chen, J., Liu, H., Liu, J., Qi, J., Wei, B., Yang, J., Liang, H., Chen, Y., Chen, J., Wu, Y., et al. (2013). H3K9 methylation is a barrier during somatic cell reprogramming into iPSCs. Nat. Genet. *45*, 34–42.

De Bonis, M.L., Cerase, A., Matarazzo, M.R., Ferraro, M., Strazzullo, M., Hansen, R.S., Chiurazzi, P., Neri, G., and D'Esposito, M. (2006). Maintenance of X- and Y-inactivation of the pseudoautosomal (PAR2) gene SPRY3 is independent from DNA methylation and associated to multiple layers of epigenetic modifications. Hum. Mol. Genet. *15*, 1123–1132.

Esteban, M.A., Wang, T., Qin, B., Yang, J., Qin, D., Cai, J., Li, W., Weng, Z., Chen, J., Ni, S., et al. (2010). Vitamin C enhances the generation of mouse and human induced pluripotent stem cells. Cell Stem Cell *6*, 71–79.

Fernando, R.I., Litzinger, M., Trono, P., Hamilton, D.H., Schlom, J., and Palena, C. (2010). The T-box transcription factor Brachyury promotes epithelial-mesenchymal transition in human tumor cells. J. Clin. Invest. *120*, 533–544.

Fico, A., Manganelli, G., Simeone, M., Guido, S., Minchiotti, G., and Filosa, S. (2008). High-throughput screening-compatible-single-step protocol to differentiate embryonic stem cells in neurons. Stem Cells Dev. *17*, 573–584.

Folmes, C.D., Dzeja, P.P., Nelson, T.J., and Terzic, A. (2012). Metabolic plasticity in stem cell homeostasis and differentiation. Cell Stem Cell *11*, 596–606.

Giannone, G., Dubin-Thaler, B.J., Rossier, O., Cai, Y., Chaga, O., Jiang, G., Beaver, W., Döbereiner, H.G., Freund, Y., Borisy, G., and Sheetz, M.P. (2007). Lamellipodial actin mechanically links myosin activity with adhesion-site formation. Cell *128*, 561–575.

Imuta, Y., Nishioka, N., Kiyonari, H., and Sasaki, H. (2009). Short limbs, cleft palate, and delayed formation of flat proliferative chondrocytes in mice with targeted disruption of a putative protein kinase gene, Pkdcc (AW548124). Dev. Dyn. *238*, 210–222.

Jiang, J., Chan, Y.S., Loh, Y.H., Cai, J., Tong, G.Q., Lim, C.A., Robson, P., Zhong, S., and Ng, H.H. (2008). A core Klf circuitry regulates self-renewal of embryonic stem cells. Nat. Cell Biol. *10*, 353–360.

Kalluri, R. (2009). EMT: when epithelial cells decide to become mesenchymal-like cells. J. Clin. Invest. *119*, 1417–1419.

Katada, S., Imhof, A., and Sassone-Corsi, P. (2012). Connecting threads: epigenetics and metabolism. Cell *148*, 24–28.

Kinoshita, M., Era, T., Jakt, L.M., and Nishikawa, S. (2009). The novel protein kinase Vlk is essential for stromal function of mesenchymal cells. Development *136*, 2069–2079.

Li, R., Liang, J., Ni, S., Zhou, T., Qing, X., Li, H., He, W., Chen, J., Li, F., Zhuang, Q., et al. (2010). A mesenchymal-to-epithelial transition initiates and is required for the nuclear reprogramming of mouse fibroblasts. Cell Stem Cell *7*, 51–63.

Liu, W., Le, A., Hancock, C., Lane, A.N., Dang, C.V., Fan, T.W., and Phang, J.M. (2012). Reprogramming of proline and glutamine metabolism contributes to the proliferative and metabolic responses regulated by oncogenic transcription factor c-MYC. Proc. Natl. Acad. Sci. USA *109*, 8983–8988.

Loh, Y.H., Zhang, W., Chen, X., George, J., and Ng, H.H. (2007). Jmjd1a and Jmjd2c histone H3 Lys 9 demethylases regulate self-renewal in embryonic stem cells. Genes Dev. *21*, 2545–2557.

Mali, P., Chou, B.K., Yen, J., Ye, Z., Zou, J., Dowey, S., Brodsky, R.A., Ohm, J.E., Yu, W., Baylin, S.B., et al. (2010). Butyrate greatly enhances derivation of human induced pluripotent stem cells by promoting epigenetic remodeling and the expression of pluripotency-associated genes. Stem Cells *28*, 713–720.

Parisi, S., D'Andrea, D., Lago, C.T., Adamson, E.D., Persico, M.G., and Minchiotti, G. (2003). Nodal-dependent Cripto signaling promotes cardiomyogenesis and redirects the neural fate of embryonic stem cells. J. Cell Biol. *163*, 303–314.

Phang, J.M., Pandhare, J., and Liu, Y. (2008). The metabolism of proline as microenvironmental stress substrate. J. Nutr. *138*, 2008S–2015S.

Phang, J.M., Liu, W., Hancock, C., and Christian, K.J. (2012). The proline regulatory axis and cancer. Front. Oncol. *2*, 60.

Phang, J.M., Liu, W., and Hancock, C. (2013). Bridging epigenetics and metabolism: role of non-essential amino acids. Epigenetics *8*, 231–236.

Ridley, A.J. (2011). Life at the leading edge. Cell *145*, 1012–1022.

Samavarchi-Tehrani, P., Golipour, A., David, L., Sung, H.K., Beyer, T.A., Datti, A., Woltjen, K., Nagy, A., and Wrana, J.L. (2010). Functional genomics reveals a BMP-driven mesenchymal-to-epithelial transition in the initiation of somatic cell reprogramming. Cell Stem Cell *7*, 64–77.

Sarkar, D., Shields, B., Davies, M.L., Müller, J., and Wakeman, J.A. (2012). BRACHYURY confers cancer stem cell characteristics on colorectal cancer cells. Int. J. Cancer *130*, 328–337.

Sassone-Corsi, P. (2013). Physiology. When metabolism and epigenetics converge. Science *339*, 148–150.

Scott, D.A., Richardson, A.D., Filipp, F.V., Knutzen, C.A., Chiang, G.G., Ronai, Z.A., Osterman, A.L., and Smith, J.W. (2011). Comparative metabolic flux profiling of melanoma cell lines: beyond the Warburg effect. J. Biol. Chem. *286*, 42626–42634.

Shyh-Chang, N., Locasale, J.W., Lyssiotis, C.A., Zheng, Y., Teo, R.Y., Ratanasirintrawoot, S., Zhang, J., Onder, T., Unternaehrer, J.J., Zhu, H., et al. (2013). Influence of threonine metabolism on S-adenosylmethionine and histone methylation. Science *339*, 222–226.

Tesar, P.J., Chenoweth, J.G., Brook, F.A., Davies, T.J., Evans, E.P., Mack, D.L., Gardner, R.L., and McKay, R.D. (2007). New cell lines from mouse epiblast share defining features with human embryonic stem cells. Nature *448*, 196–199.

Thiery, J.P., Acloque, H., Huang, R.Y., and Nieto, M.A. (2009). Epithelial-mesenchymal transitions in development and disease. Cell *139*, 871–890.

Wang, J., Alexander, P., Wu, L., Hammer, R., Cleaver, O., and McKnight, S.L. (2009). Dependence of mouse embryonic stem cells on threonine catabolism. Science *325*, 435–439.

Wang, T., Chen, K., Zeng, X., Yang, J., Wu, Y., Shi, X., Qin, B., Zeng, L., Esteban, M.A., Pan, G., and Pei, D. (2011). The histone demethylases Jhdm1a/1b enhance somatic cell reprogramming in a vitamin-C-dependent manner. Cell Stem Cell *9*, 575–587.

Washington, J.M., Rathjen, J., Felquer, F., Lonic, A., Bettess, M.D., Hamra, N., Semendric, L., Tan, B.S., Lake, J.A., Keough, R.A., et al. (2010). L-Proline induces differentiation of ES cells: a novel role for an amino acid in the regulation of pluripotent cells in culture. Am. J. Physiol. Cell Physiol. *298*, C982–C992.

Yanes, O., Clark, J., Wong, D.M., Patti, G.J., Sánchez-Ruiz, A., Benton, H.P., Trauger, S.A., Desponts, C., Ding, S., and Siuzdak, G. (2010). Metabolic oxidation regulates embryonic stem cell differentiation. Nat. Chem. Biol. *6*, 411–417.

Yang, J., and Weinberg, R.A. (2008). Epithelial-mesenchymal transition: at the crossroads of development and tumor metastasis. Dev. Cell *14*, 818–829.

Yang, L., Soonpaa, M.H., Adler, E.D., Roepke, T.K., Kattman, S.J., Kennedy, M., Henckaerts, E., Bonham, K., Abbott, G.W., Linden, R.M., et al. (2008). Human cardiovascular progenitor cells develop from a KDR+ embryonic-stem-cell-derived population. Nature *453*, 524–528.

Zarse, K., Schmeisser, S., Groth, M., Priebe, S., Beuster, G., Kuhlow, D., Guthke, R., Platzer, M., Kahn, C.R., and Ristow, M. (2012). Impaired insulin/IGF1 signaling extends life span by promoting mitochondrial L-proline catabolism to induce a transient ROS signal. Cell Metab. *15*, 451–465.

Zhang, J., Nuebel, E., Daley, G.Q., Koehler, C.M., and Teitell, M.A. (2012). Metabolic regulation in pluripotent stem cells during reprogramming and self-renewal. Cell Stem Cell *11*, 589–595.